Archives of Biochemistry and Biophysics 761 (2024) 110179

Contents lists available at ScienceDirect

Archives of Biochemistry and Biophysics

journal homepage: www.elsevier.com/locate/yabbi

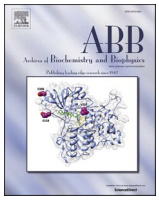

Critical aggregation concentration and reversibility of amyloid-β (1–40) oligomers

Sara Illodo [a,b], Wajih Al-Soufi [a], Mercedes Novo [a,*]

[a] Facultade de Ciencias, Departamento de Química Física, Campus Terra, Universidade de Santiago de Compostela, 27002, Lugo, Spain
[b] Centro Singular de Investigación en Química Biolóxica e Materiais Moleculares (CiQUS) and Facultade de Química, Departamento de Química Física, Universidade de Santiago de Compostela, 15782, Santiago de Compostela, Spain

ARTICLE INFO

Keywords:
Amyloid aggregation
Amyloid-β 1–40
Fluorescence correlation spectroscopy

ABSTRACT

Amyloid-beta (Aβ) aggregation is a critical factor in the pathogenesis of Alzheimer's disease, with distinct aggregation behaviours observed between its isoforms Amyloid-β 1–40 (Aβ40) and 1–42 (Aβ42). In this study, we investigated the aggregation properties of Aβ40 using fluorescence correlation spectroscopy (FCS) and detailed data analysis. Our results reveal that Aβ40 undergoes a two-step cooperative aggregation process. The first step, characterized by a critical aggregation concentration (*cac*) of 0.5 ± 0.3 μM, results in the formation of metastable oligomers of 5–25 monomers and stable oligomers of 50–100 monomers, with less than 10 % of the total amyloid aggregated. The second step, with a *cac* of 19 ± 2 μM, leads to the formation of much larger aggregates, consistent with protofibrils, and approximately 50 % aggregated amyloid. Notably, the *cac* for Aβ40 is significantly higher, and the fraction of aggregated amyloid is much lower compared to Aβ42, indicating a lower propensity for aggregation. Additionally, our findings suggest that Aβ40 early oligomers are reversible upon dilution, albeit with a kinetic barrier to disaggregation. These insights into the aggregation mechanisms of Aβ40 enhance our understanding of its role in Alzheimer's disease and may inform therapeutic strategies targeting amyloid aggregation.

1. Introduction

Understanding neurodegenerative diseases remains a prominent and expanding field of research due to their significant impact on public health. Alzheimer's disease (AD) is a major disorder within this category and continues to be incompletely understood. Several hypotheses regarding its causes are currently under debate, primarily focusing on the role of tau protein and amyloid peptides [1–5]. The most widely accepted one is the 'amyloid cascade hypothesis,' which identifies amyloid peptide aggregation as a detrimental factor for AD [3,6,7]. Amyloid peptides are intrinsically disordered proteins with a high propensity for aggregation. During this process several species such as dimers, trimers, oligomers and protofibrils are formed. It is widely believed that the neurotoxic species triggering AD are not the final fibrils, but the early-stage species such as oligomers and protofibrils [8–12].

Among the different amyloid peptides, amyloid-β (1–40) and (1–42) (Aβ40 and Aβ42, respectively) are identified as the main precursors of AD. Even though their sequences differ only in the last two amino acids, their properties vary significantly. Aβ40, the most abundant peptide (representing 80–90 %), has higher solubility and a lower tendency to aggregate compared to Aβ42. Due to its higher aggregation propensity, Aβ42 has been the primary focus of study. However, research indicates that aggregation mechanisms vary with sequence length, cross-interactions among different peptides, extrinsic physicochemical factors and interactions with lipid membranes and metal ions [12–23]. This requires a multidisciplinary approach to the aggregation process to understand its mechanism and characterize the aggregates formed and their toxicity [12,24,25].

Given that Aβ40 is the predominant species in the organism, deciphering its aggregation mechanism seems crucial. But the literature on Aβ40 aggregation reveals significant discrepancies. Some authors suggest that Aβ40 aggregation leads directly to fibrils without forming oligomers or protofibrils [20,21]. In contrast, others report results that hint at an early aggregation leading to oligomer formation [17,18,26–31], though there are inconsistencies in the reported sizes of these oligomers [17,28,31,32]. The lack of reproducibility in amyloid aggregation studies is intrinsic to the self-association process itself, stochastic and autocatalytic, and is aggravated by the difficulty of obtaining

* Corresponding author.
E-mail address: m.novo@usc.es (M. Novo).

https://doi.org/10.1016/j.abb.2024.110179
Received 16 July 2024; Received in revised form 13 September 2024; Accepted 9 October 2024
Available online 10 October 2024

completely monomeric starting samples and the presence of impurities [12].

Our objective is an *in vitro* quantitative study of the early aggregation of Aβ40 starting from monomeric samples and the comparison with our previously reported results for Aβ42 [33,34]. In previous studies we found that Aβ42 aggregates only when the concentration of amyloid monomers exceeds the critical aggregation concentration (*cac*) of 91 ± 14 nmol/L [33]. This spontaneous, cooperative process resembles surfactant self-assembly and yields stable micelle-like oligomers whose size (≈50 monomers, $R_h \approx 7.3$ nm–10.7 nm) and elongated shape are independent of incubation time and peptide concentration. These results for the oligomers are in very good agreement with the reported micellar assemblies of several amyloid peptides [26,29,35,36]. In general, these studies show relatively high values of critical aggregation concentrations, which are affected by the sensitivity of the technique and the strong adsorption of amyloids that influences the real concentration in solution [37].

We employ Fluorescence Correlation Spectroscopy (FCS), a technique that provides information about the number and size of freely diffusing particles in solution. FCS allows us to monitor the fraction of both aggregates and monomers in solution and to determine the size distribution of the aggregates as a function of peptide concentration and time. Additionally, FCS enables the determination of the true total amyloid concentration, which is a critical parameter in quantitative aggregation studies due to the strong adsorption of the peptides to interfaces [37]. Using this information, we aim to determine the *cac* of Aβ40 oligomerization and to study the reversibility and stability of the aggregates.

2. Experimental section

2.1. Materials

This study utilized both fluorescently labelled (Aβ40*) and unlabelled (Aβ40) commercial amyloid-β 1–40. The labelled HiLyte Fluor 488-β-amyloid(1–42) was obtained from Anaspec Inc. with a purity of ≥95 % while the unlabelled amyloid was purchased from Genscript USA Inc. To prevent contamination, aliquoted 1,1,1,3,3,3-hexafluoro-2-propanol (HFIP) ≥99 % from Sigma Aldrich was used. Aqueous solutions under physiological conditions were prepared using PBS (pH 7.5, ionic strength 0.18 M, phosphate concentration 13 mM and salt concentration of 142 mM sodium and 2.7 mM potassium) as the buffer.

2.2. Preparation of monomeric amyloid

To ensure the amyloid peptide samples were initially free of aggregates, the disaggregation procedure reported by Stine et al. [38,39] was applied as first step of the sample preparation for both labelled and unlabelled commercial peptides.

The amyloid was dissolved in HFIP at a concentration of not exceeding 1 mg/mL. This solution was then incubated at room temperature for 1 h with occasional mixing, followed by 20 min of continuous shaking. This solution was then aliquoted into several vials, and the HFIP was evaporated under a stream of nitrogen. The vials were transferred into a desiccator and subjected to vacuum for 3 h to remove any remaining traces of HFIP. The resulting dried aliquots of monomeric Aβ40 were sealed and stored at −20 °C.

2.3. Sample preparation

All samples were prepared maintaining the concentration of labelled amyloid around 20 nM while changing the concentration of the unlabelled peptide. Different procedures were applied depending on the specific objectives of each experiment.

2.3.1. Independent samples for aggregation studies

These samples were prepared individually to investigate the potential dependence of the aggregation process on the incubation time and to obtain independent measurements for each concentration, as reported in previous studies [33,34].

First, an aliquot of dry monomeric labelled amyloid was dissolved in PBS to achieve the desired concentration of about 20 nM. After verifying the absence of aggregates by measuring a FCS curve, this solution was used to directly dissolve an aliquot of the unlabelled peptide. The final solution was then mixed thoroughly at room temperature for 5 min and used for FCS measurements. The concentration of unlabelled amyloid was varied from 0 to 32 μM.

2.3.2. Samples for reversibility studies

Reversibility of the aggregation process was studied by dilution of concentrated amyloid samples covering peptide concentrations ranging from 150 μM to 0.5 μM, divided into three series with nominal concentration ranges of 0.5–25 μM, 5–100 μM, and 50–150 μM.

For each series, the sample of the highest concentration was prepared as described above for the individual samples. Diluted samples were then prepared directly in the microplate well during the FCS experiment using an extraction-dilution method. A small volume was extracted from the total sample volume of 100 μL and replaced with the same volume of a solution containing the same concentration of labelled amyloid but no unlabelled peptide. This method ensured the concentration of labelled amyloid and the sample volume remained constant while the unlabelled amyloid was diluted. The sample was mixed in the well by repeated pipetting. FCS curves were measured for the solutions obtained at each step within few minutes after dilution. These extraction-dilution-measurement cycles were repeated to cover the desired concentration range.

2.3.3. Samples for time stability studies

For the stability studies, the independent samples from the aggregation studies were stored at room temperature. For short incubation times, they were kept in the well plate covered with Parafilm sealing film and a silicone sealing mat to avoid evaporation and contamination. FCS curves were measured every 10–20 min for 2 h. For longer incubation times the same samples were stored in microcentrifuge tubes for the desired incubation period and then transferred to the well plate for FCS measurements.

2.4. Fluorescence correlation spectroscopy

For FCS experiments 100 μL of the sample were placed into a well of a 96-well glass-bottom microplate (Whatman Ltd) and allowed to equilibrate for approximately 5 min to achieve a constant temperature. All measurements were conducted at room temperature (21.5 ± 0.5 °C). The FCS setup, previously described [40,41], is summarized in the SI. For each sample, several correlation curves, each consisting of 5 million photons, were recorded to ensure high-quality data.

The FCS focus volume ($V = 0.52 \pm 0.04$ μm^3, radial width $\omega_{xy} = 0.27 \pm 0.01$ μm) was calibrated using Rhodamine 123 as reference dye, with a diffusion coefficient $D_{R123} = (4.7 \pm 0.3) \times 10^{-10}$ m^2 s^{-1} at 25 °C derived from multiple literature sources [42–44]. For the calculation of the diffusion coefficients, temperature effects were taking into account using Stokes-Einstein relation.

From power series of monomeric and aggregated samples of the peptide (Figure SI1) an excitation power of 30 μW, corresponding to an irradiance of 24 kW cm^{-2} was selected to prevent photobleaching.

2.5. Data analysis

We applied a specific data analysis procedure developed by our group for Aβ42 to extract quantitative information on the conformation and size of the aggregates as well as on the degree of aggregation [33,

34]. In the following discussion we make reference to the analysis steps briefly described in the Data Analysis section of the SI, which includes a theoretical background explanation followed by a description of the data analysis procedure applied to the experimental data. This analysis yields the degree of aggregation as a function of concentration, the aggregation number and scaling factor of the oligomers, and the true total amyloid concentration.

To determine the critical aggregation concentrations from the observed dependence of the degree of aggregation on the total amyloid concentration, we adapted the aggregation concentration model initially derived by our group for surfactant micelle formation [45] to the case of two independent aggregation processes (see equation SI45).

3. Results and discussion

3.1. Monomeric Aβ40 characterization

First, we characterized the monomeric Aβ40 to confirm that the starting peptide samples were free of aggregates. FCS measurements of samples of low concentrations of labelled amyloid (Aβ40*) fit well with a single diffusion term (eq. SI1), yielding a diffusion time of 151 ± 2 μs, and a value of the diffusion coefficient of monomeric Aβ40 of (1.30 ± 0.14) × 10^{-10} m^2 s^{-1} at 25 °C. This value is consistent with that obtained for monomeric Aβ42 [33], (1.27 ± 0.09) × 10^{-10} m^2 s^{-1} at 25 °C converted to the R123 reference value used in this work. Both values follow the relative molar mass dependency $D \sim M^{\nu}$ with a value of $\nu = 0.44$ as determined by Danielsson et al. [46] for a series of amyloid peptides using PFG-NMR.

Comparing the absolute diffusion coefficients, our values of labelled monomeric amyloids are approximately 10 % lower than those reported by Danielsson et al. [46], a difference within the uncertainty range primarily due to the uncertainty of the reference value. This discrepancy may also arise from a potential change in the scaling factor ν in the labelled amyloids due to the fluorophore or to the presence of small amounts of dimers in the samples. A dimer would have a diffusion coefficient at least $2^{0.33} = 1.26$ times lower than that of the monomer, assuming a compact sphere – other shapes would lead to even higher factors [46]. Thus, Aβ40 dimers or higher assemblies would correspond to significantly smaller diffusion coefficients than those observed. We therefore conclude that our starting amyloids are indeed predominantly monomeric.

Using the Stokes-Einstein equation, we obtained a hydrodynamic radius for the Aβ40 monomer of $R_h = 1.88 \pm 0.20$ nm, which coincides within its error with that reported by our group for Aβ42 (1.93 ± 0.13 nm) [33] and with literature values found for Aβ40 monomers (ranging from 1 nm to 2 nm) [17,21,36,47].

3.2. Aggregation of Aβ – degree of aggregation

To determine the degree of aggregation, we followed the data analysis procedure described in the Supplementary Information.

The first step involved fitting the FCS curves (Step SI1) obtained for solutions with varying concentrations of unlabelled amyloid and a constant single-molecule concentration of labelled amyloid. For this Equation SI2 was globally fitted with a shared monomer diffusion time (τ_{D1}), and free diffusion times of the oligomers (τ_{D2}), relative contributions (R) and the total number of observed molecules (N).

3.2.1. Time dependency: short incubation times

To study the potential influence of the incubation time, FCS curves were recorded up to 180 min after sample preparation. For each sample, series of FCS curves were measured covering the entire observation time (Fig. 1a) and fitted with the two species model (eq. SI2) with a monomer diffusion time shared among all curves. We observed no systematic variation in the diffusion times of the aggregates (Fig. 1b) or in the relative contributions of the species (Fig. 1c), indicating that the aggregates do not grow or change during the studied time. This finding is consistent with previous observations for Aβ42 [33].

3.2.2. Brightness ratio

The fit results show that the brightness of labelled amyloid is lower in aggregates (Q_2) than in monomers (Q_1). For Aβ40* we determined a brightness ratio $q' = Q_2/Q_1 = 0.53 \pm 0.09$ (Step SI2), which coincides with the value of 0.6 ± 0.1 obtained for Aβ42 [33].

3.2.3. Aggregation number of the oligomers

From the brightness ratio q' and the monomer brightness Q_1 we obtained the mean number of labelled Aβ per aggregate $\bar{i}_u^*$ and a preliminary uncorrected mean aggregation number $\bar{n}_u$ of each experiment (Step SI3). The double-logarithmic plot of the diffusion time ratios τ_{D2}/τ_{D1} versus $\bar{n}_u$ (Figure SI2) yields a scaling factor of the aggregates $\nu_2 =$

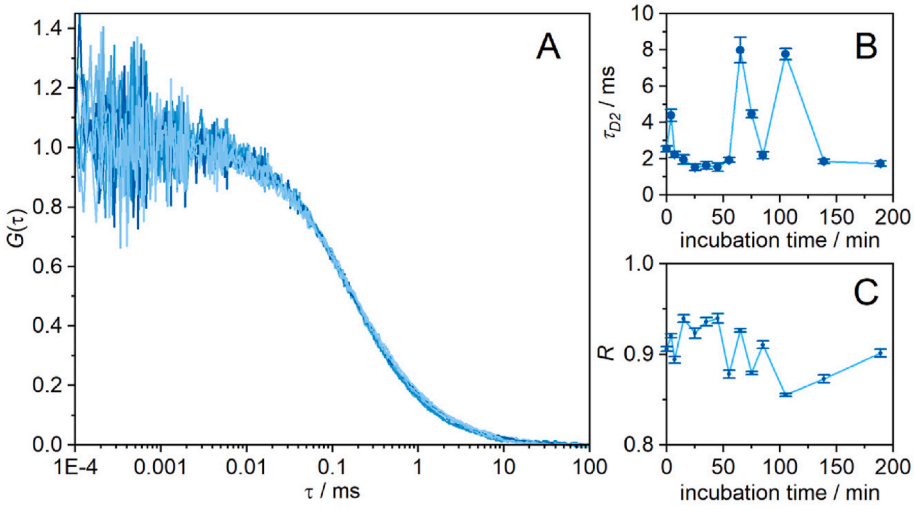

Fig. 1. Panel A: Normalized FCS curves of a given amyloid sample (nominal total amyloid concentration 4 μM) recorded during 180 min at the incubation times indicated in panels B and C. Panel B: Diffusion times of the aggregates, τ_{D2}, obtained from global fits of eq. SI2 to the FCS curves shown in Panel A as a function of incubation time. The monomer diffusion time, τ_{D1}, was fixed to the value obtained for monomeric Aβ40. Panel C: Factor R representing the relative contribution of monomeric amyloids to the FCS curves obtained from each of the curves shown in Panel A over the incubation time. The FCS curves in panel A were normalized using the value of N obtained from the fits.

0.71 ± 0.07 (Step SI4). This relatively high value indicates a shift from the random coil conformation of the monomer to a more elongated, fibril-like conformation of the early aggregates. Such a conformation was already observed in the case of Aβ42 ($\nu = 0.75$) [33] and is in good agreement with the reported spherocylindrical geometry of Aβ40 micellar assemblies determined from small angle neutron scattering [26].

Using the results of the previous step, we calculate a new corrected aggregation number $\bar{n}_c$ for each measurement (Step SI5). Figure SI3 shows the corrected mean aggregation number as a function of the nominal total Aβ40 concentration. No systematic variation of the aggregation numbers with the incubation time or the total amyloid concentration is observed, consistent with the findings for Aβ42 [33]. Mean aggregation numbers range between approximately 10 and 200, although some values fall outside this range with high uncertainties, especially in the dilution series. We further analyse the size of the aggregates below.

3.2.4. Degree of aggregation

Next, we analyse the fraction of the total amyloid that is aggregated (degree of aggregation γ) as a function of the total true Aβ40 concentration. The procedure is described in Steps S5 and S6 of the SI. Due to the high tendency of amyloids to adsorb to surfaces, determining the true amyloid concentration is crucial in this analysis, although for Aβ40 a much better correlation between nominal and true concentrations than for Aβ42 is observed (Figure SI4) [33].

Fig. 2 shows the degree of aggregation determined from individually prepared samples as a function of the total true Aβ40 concentrations (depicted by orange circles in Fig. 2, nominal concentrations ranging from 0.005 μM to 43 μM). The fraction of aggregated amyloid depends strongly on the total Aβ40 concentration, revealing three distinct regions. Below 0.1 μM minimal aggregation is observed. Between 0.1 μM and 10 μM, the degree of aggregation rises, reaching up to 10 % of the total Aβ40. Above 10 μM, the degree of aggregation increases markedly.

The dilution series that we discuss in more detail in the following section, provides data for the degree of aggregation at higher Aβ40 concentrations, not reached in the individually prepared samples. As shown in Fig. 2, at concentrations higher than 10 μM, the degree of aggregation increases further from values of $\gamma \approx 0.05$–0.1 to around 0.5, corresponding to roughly 50 % of aggregated Aβ40 above 100 μM. A very good agreement is observed between the different types of samples.

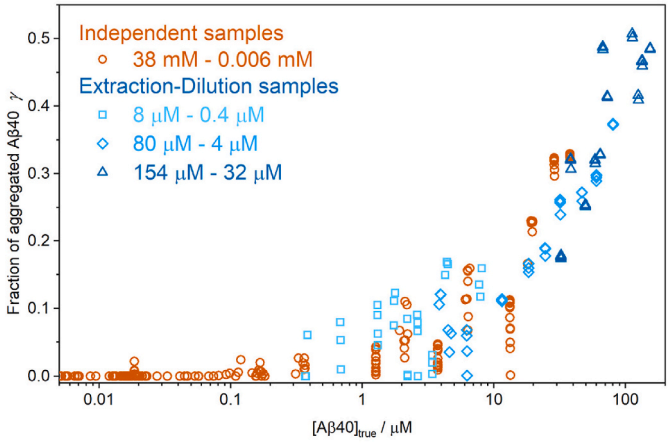

Fig. 2. Degree of aggregation γ of Aβ40 samples, determined using the procedure outlined in the SI, plotted against the true total amyloid concentration in solution. Independently prepared samples are compared with series of progressively diluted samples covering the indicated nominal concentration intervals.

3.2.5. Reversibility and long-term stability

To analyse the reversibility of Aβ40 aggregation, dilution series covering the full concentration range were prepared. Fig. 2 shows the results of the degree of aggregation of these samples as a function of the true total Aβ40 concentration, together with those obtained for the independently prepared samples for comparison. It can be seen that the degree of aggregation decreases with the dilution of Aβ40, with values that overlap among the dilution series. Moreover, the degree of aggregation of samples diluted from higher concentrations decrease to the same value obtained for samples directly prepared from lower Aβ40 concentrations, hinting at an effective disaggregation of the Aβ40 oligomers. This reduction of the degree of aggregation upon dilution is accompanied by the expected increase of the relative contribution R of the monomers to the amplitude of the FCS curves (see Figure SI5). These findings suggest that the Aβ40 aggregation is reversible within the studied concentration interval.

Further studies were performed to check the stability of the samples over extended incubation periods. Figure SI6 compares data from independently prepared samples measured during 2–3 h after preparation and again after one week. No significant changes were observed in the diffusion times of the aggregates (Figures SI6 A and B) or in the relative contribution R of the monomers to the FCS curves (Figures SI6 C and D), except that for low concentrations, R values were closer to 1 after one week. This finding suggests the presence of a kinetic barrier to oligomer disaggregation, indicating that reversibility may require longer times to complete. This kinetic barrier may depend on the specific aggregation state of each oligomer. Given the dynamic nature of aggregation and disaggregation various aggregation states are likely to coexist as equilibrium is reached, which could explain the highly dispersed data in the dilution data within the range between the two *cac* values, from 0.4 to 8 μM (Fig. 2, blue squares).

The true total amyloid concentration remained constant after one week, showing no precipitation of the aggregates, which would be expected for assemblies larger than the soluble oligomers. The data collected after one week show similar standard errors of the mean values of $\tau_{D,2}$ and R, however, the uncertainties of each of individual fitted value (not shown) was much higher after one week than at the beginning of the incubation period. This suggests an increase in polydispersity as compared to the shorter incubation.

3.3. Critical aggregation concentrations

Combining all γ-values from independent samples and dilution series (Fig. 2), and calculating the mean values and uncertainties with all measurements of each sample, we obtain the data shown in Fig. 3 which will allow us to obtain the critical aggregation concentration (Step SI7). The observed variation in the degree of aggregation with the true total amyloid concentration suggests two cooperative aggregation processes at two critical aggregation concentrations. To address this, we extended the aggregation concentration model originally developed for the self-assembly of surfactants [45] to include two independent aggregations with their corresponding *cac* values, as described in the SI.

The continuous line in Fig. 3 represents the result of the weighted nonlinear fit of Equation SI45 to the experimental data. The double aggregation model fits the data well, indicating a first aggregation at $cac_1 = 0.5 \pm 0.3$ μM and a second at $cac_2 = 19 \pm 2$ μM. The corresponding transition widths ($\sigma_i = r_i \cdot cac_i$) of $\sigma_1 = 0.2$ μM and $\sigma_2 = 5.7$ μM, respectively, indicate that under the studied conditions the transition from monomeric amyloid to the first type of aggregate takes place between 0.4 and 0.7 μM, while the transition from this first oligomeric amyloid to the next one occurs in a concentration range from 13 μM to 25 μM. The fit curve also indicates that the first aggregation leads to less of 10 % of aggregated amyloid and to around 50 % well over the second *cac*, indicating that a significant fraction of Aβ40 remains monomeric even at very high amyloid concentrations.

For Aβ42, we previously found a single critical aggregation process

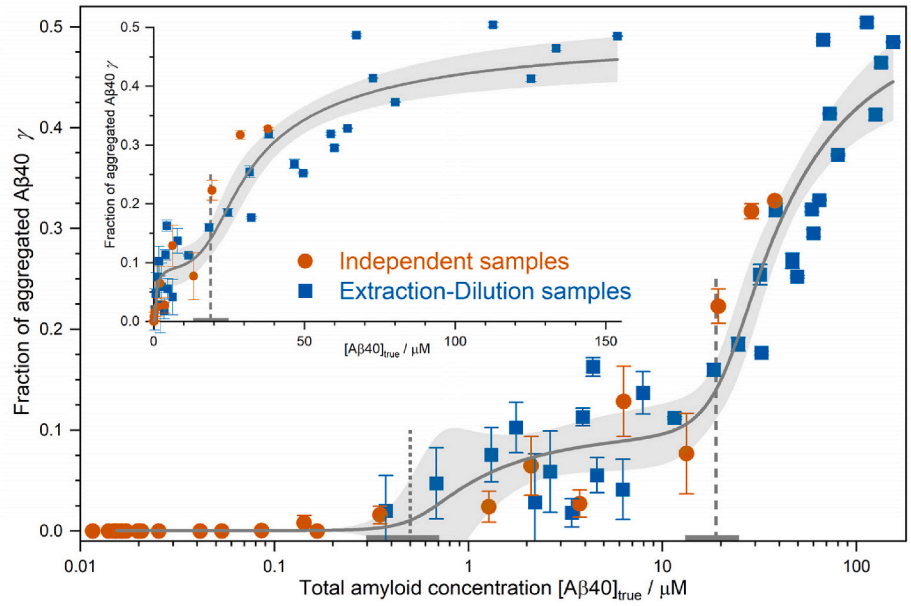

Fig. 3. Degree of aggregation of Aβ40, γ, as a function of the true total amyloid concentration in solution. The filled symbols are the mean of the γ-values shown in Fig. 2. The error bars correspond to the standard deviations. The solid line is the result of a weighted nonlinear fit of the aggregation model with a first cac of (0.5 ± 0.3) μM (vertical grey dotted line) and a second cac of (18.9 ± 2.2) μM (vertical grey dashed line) and widths of the transition regions $\sigma = r{\cdot}cac = 0.2$ μM and 5.7 μM, respectively (shaded bars around the cacs). The shaded area around the fit curve indicates 95 % confidence bands. Main Panel: logarithmic concentration scale. Inset: linear concentration scale.

with a *cac* around 0.09 μM [33]. However, the concentration ranges are significantly different in both studies. Due to the strong adsorption of Aβ42, in our previous study the true concentration of Aβ42 did not exceed 1.5 μM, about 17 times its *cac*. In contrast, the much lower tendency to adsorb of Aβ40 allowed us in this study to reach much higher concentrations (300 times the cac_1) and thus to observe different aggregation processes not visible in the previous study.

The cac_1 of Aβ40 is approximately 5 times higher than that of Aβ42, in accordance with the increased probability of dimerization of ab42 as an initial step of aggregation [23]. However, when comparing a concentration range up to 17 × cac_1, the behaviour of Aβ40 is very similar to that of Aβ42. Below the *cac,* only small or no aggregates are found. Above it, stable aggregates with a relatively narrow size distribution are formed. For Aβ42, no further aggregation process was found due to the limited concentration range. In contrast, for Aβ40, a second aggregation process was observed above the cac_2 (≈25 × cac_1), resulting in much bigger aggregates. This second aggregation can be explained by the further growth of the initial oligomers to form protofibrils, as described in the literature [21].

The higher cac_1 of Aβ40 and its much lower degree of aggregation compared to Aβ42 align with its significantly lower tendency to aggregate. Moreover, this significant difference in the aggregation behaviour could be underestimated since, in contrast to the Aβ40 samples used in this work, the Aβ42 samples for oligomerization studies were treated with DMSO prior to solubilization with PBS [33], possibly leading to a somewhat higher cac of Aβ42.

Compared to literature data, the cac_2 of Aβ40 determined in this work is close to the value of 35 μM reported by Yong et al. [26]. The low degree of aggregation could also explain the mechanism proposed for Aβ40 of direct fibril formation [21].

3.4. Size distribution of the aggregates

We estimate the size distribution of the aggregates from the histogram of the mean aggregation number of the oligomers shown in Fig. 4 (Step SI8). The histogram reveals a high number of very small aggregates with $\bar{n} < 30$, and a second population with higher aggregation

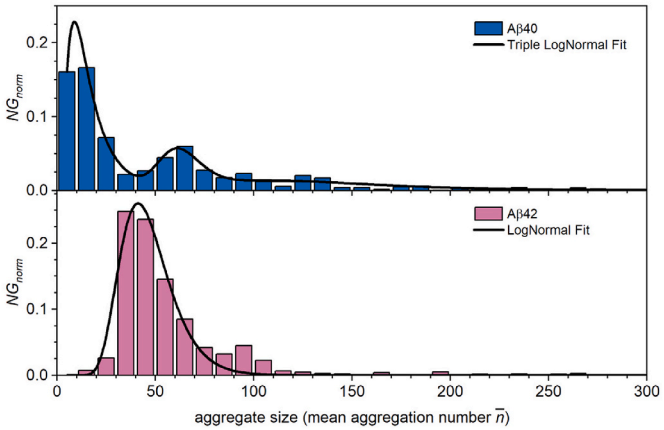

Fig. 4. *Size distribution of Aβ aggregates. Upper panel: Histogram of the mean aggregation number obtained from all Aβ40 samples at different amyloid concentrations. The curve corresponds to the fit of a triple Lognormal distribution with* $\bar{n}_{mean,1} = 14$, $\bar{n}_{mean,2} = 62$, *and* $\bar{n}_{mean,3} = 128$. *Lower panel: Histogram of Aβ42 aggregates recalculated with data from Ref.* [33]. *The curve corresponds to the fit of a Lognormal distribution with* $\bar{n}_{mean} = 45$.

numbers between 40 and 80. Furthermore, a small number of much bigger aggregates were observed, with sizes up to several hundreds of monomers. The number of these big aggregates is clearly underestimated due to limitations of the FCS experiment.

Fitting the histogram with a triple log-normal distribution, we obtain a first group of small aggregates of 5–25 monomers ($\bar{n}_{mean,1} = 14$) and a second wider group with 40–80 monomers ($\bar{n}_{mean,2} = 62$) per aggregate. The third distribution represents much bigger aggregates.

To relate this size distribution to the double aggregation process deduced from the degree of aggregation (Fig. 3) we constructed separate size histograms from samples with very low and very high true Aβ40 concentrations (Figure SI7). Below the first critical aggregation concentration (cac_1), only small aggregates were found (Figure SI7A). Once the cac_1 is reached a relatively homogeneous population of aggregates

with $\overline{n} = 62$ forms. Well above the second aggregation concentration mostly much bigger aggregates are observed with a very wide size distribution (Figure SI7B).

A possible interpretation of these findings is that during the first aggregation at cac_1 a small fraction of the monomeric Aβ40 forms stable oligomers with predominantly $\overline{n} = 62$ and a much lower amount of metastable oligomers with $\overline{n} = 14$, which convert into the former as concentration increases. At higher concentrations, above cac_2, these oligomers coalesce and/or seed much bigger aggregates involving a much higher fraction of the amyloid. In fact, at the studied higher concentrations, the critical aggregation model used for the fitting may underestimate the degree of aggregation, which may increase to much higher values than the model indicates. Experiments with much higher amyloid concentration would be needed to confirm one or the other prediction.

Focusing on the smaller oligomers, their aggregation numbers correspond to values of the hydrodynamic radius around 4 nm for the metastable aggregates and 12 nm for the larger ones. These results are in very good agreement with the reported micelle-like oligomers of Aβ40 with hydrodynamic radii around 5 nm at 120 min (metastable) and 10–20 nm at 720 min [29]. Additionally, two populations of low (0.9 nm $< R_h <$ 5 nm) and higher (5 nm $< R_h <$ 50 nm) molar mass were observed by Deleanu et al. [21], with a very small percentage of the total amyloid, which is consistent with the low fraction of aggregated amyloid that we observed in the first aggregation step.

In contrast, in our study of the early aggregation of Aβ42 [33], we only observed the oligomer species with larger aggregation number around 50 and hydrodynamic radius between 7.3 nm and 10.7 nm. This difference was also reported by Morel et al. [29], who found only stable oligomers around 15 nm. The different behavior in the size distribution of the aggregates of the two amyloids could be related to the more pronounced conformational change of Aβ40 during the aggregation process [29].

In relation to the longer aggregates observed in Aβ40, especially above cac_2, their mean hydrodynamic radius would be around 20 nm and its size would increase with time, in good agreement with what is described in the bibliography [29]. In the case of Ab42, these types of aggregates were hardly observed, which may be due to the much lower true concentration of amyloid in those experiments [33].

4. Conclusions

In this study, we have systematically investigated the aggregation behaviour of Aβ40 using fluorescence correlation spectroscopy (FCS). Our results reveal a two-step cooperative aggregation process for Aβ40, which contrasts with the single-step aggregation observed for Aβ42.

The first critical aggregation concentration (cac_1) for Aβ40 is approximately 0.5 ± 0.3 μM, about five times higher than that of Aβ42. Below this concentration, no significant aggregation is observed. Surpassing cac_1, small metastable oligomers of about 14 monomers and stable oligomers of 62 monomers form, together not exceeding 10 % of the total Aβ40 concentration. These stable aggregates are similar in size and shape to those observed in Aβ42, but the higher *cac* and the much lower fraction of aggregated amyloid highlight Aβ40's much lower aggregation tendency.

A second critical aggregation concentration (cac_2) at 19 ± 2 μM leads to the formation of much larger aggregates, possibly protofibrils, with around 50 % aggregated amyloid. This demonstrates the potential for further growth of initial oligomers at higher concentrations.

The transition widths for these aggregation steps indicate relatively narrow concentration ranges in which these processes occur, underscoring the distinct stages of Aβ40 aggregation.

Our results suggest that early Aβ40 oligomers are reversible upon dilution, although a kinetic barrier may exist, implying that longer times are required for complete reversibility.

Our comparative analysis shows that while Aβ40 and Aβ42 share some similarities in their aggregation behaviour, Aβ40 has a markedly lower aggregation tendency. This is evidenced by its higher cac_1 and lower degree of aggregation. Finally, the stability studies indicate that Aβ40 oligomers remain stable over time, with no significant changes in aggregate size or composition after one week, although an increase in polydispersity is noted. This stability, combined with the higher aggregation threshold, further underscores the distinct aggregation dynamics of Aβ40 compared to Aβ42.

Our findings provide a deeper understanding of the aggregation mechanisms of Aβ40 and highlight the importance of concentration and incubation time in studying amyloid aggregation. These insights could inform therapeutic strategies targeting amyloid aggregation in Alzheimer's disease.

CRediT authorship contribution statement

Sara Illodo: Writing – original draft, Visualization, Investigation, Data curation. **Wajih Al-Soufi:** Writing – review & editing, Visualization, Software, Methodology, Formal analysis, Conceptualization. **Mercedes Novo:** Writing – review & editing, Supervision, Resources, Project administration, Methodology, Funding acquisition, Conceptualization.

Declaration of competing interest

The authors declare that they have no known competing financial interests or personal relationships that could have appeared to influence the work reported in this paper.

Acknowledgments

We thank the Spanish Ministerio de Ciencia e Innovación and the Xunta de Galicia for their financial support (PID2020-120378RB-I00, ED431B 2019/18). S.I. thanks the Xunta de Galicia for her research scholarship, grant number ED481A2021/211.

Appendix A. Supplementary data

Supplementary data to this article can be found online at https://doi.org/10.1016/j.abb.2024.110179.

References

[1] M.P. Murphy, H. LeVine, Alzheimer's disease and the β-amyloid peptide, J. Alzheimers Dis. JAD 19 (2010) 311, https://doi.org/10.3233/JAD-2010-1221.
[2] J.C. Lee, S.J. Kim, S. Hong, Y.S. Kim, Diagnosis of Alzheimer's disease utilizing amyloid and tau as fluid biomarkers, Exp. Mol. Med. 515 (51) (2019) 1–10, https://doi.org/10.1038/s12276-019-0250-2, 2019.
[3] H. Hampel, J. Hardy, K. Blennow, C. Chen, G. Perry, S.H. Kim, V.L. Villemagne, P. Aisen, M. Vendruscolo, T. Iwatsubo, C.L. Masters, M. Cho, L. Lannfelt, J. L. Cummings, A. Vergallo, The amyloid-β pathway in alzheimer's disease, Mol. Psychiatr. 26 (2021) 5481–5503, https://doi.org/10.1038/s41380-021-01249-0.
[4] S. Wegmann, J. Biernat, E. Mandelkow, A current view on Tau protein phosphorylation in Alzheimer's disease, Curr. Opin. Neurobiol. 69 (2021) 131–138, https://doi.org/10.1016/j.conb.2021.03.003.
[5] A.R. Roda, G. Serra-Mir, L. Montoliu-Gaya, L. Tiessler, S. Villegas, Amyloid-beta peptide and tau protein crosstalk in Alzheimer's disease, Neural Regen. Res. 17 (2022) 1666–1674, https://doi.org/10.4103/1673-5374.332127.
[6] P.T. Lansbury, H.A. Lashuel, A century-old debate on protein aggregation and neurodegeneration enters the clinic, Nature 443 (2006) 774–779, https://doi.org/10.1038/NATURE05290.
[7] J. Hardy, N. Bogdanovic, B. Winblad, E. Portelius, N. Andreasen, A. Cedazo-Minguez, H. Zetterberg, Pathways to Alzheimer's disease, J. Intern. Med. 275 (2014) 296–303.
[8] G.P. Lotz, J. Legleiter, The role of amyloidogenic protein oligomerization in neurodegenerative disease, J. Mol. Med. 91 (2013) 653–664, https://doi.org/10.1007/s00109-013-1025-1.
[9] S.J.C. Lee, E. Nam, H.J. Lee, M.G. Savelieff, M.H. Lim, Towards an understanding of amyloid-β oligomers: characterization, toxicity mechanisms, and inhibitors, Chem. Soc. Rev. 46 (2017) 310–323, https://doi.org/10.1039/C6CS00731G.
[10] M. Tolar, S. Abushakra, M. Sabbagh, The path forward in Alzheimer's disease therapeutics: reevaluating the amyloid cascade hypothesis, Alzheimers Dement (2019), https://doi.org/10.1016/j.jalz.2019.09.075.

[11] P. Madhu, S. Mukhopadhyay, Distinct types of amyloid-β oligomers displaying diverse neurotoxicity mechanisms in Alzheimer's disease, J. Cell. Biochem. 122 (2021) 1594–1608, https://doi.org/10.1002/jcb.30141.
[12] P.H. Nguyen, A. Ramamoorthy, B.R. Sahoo, J. Zheng, P. Faller, J.E. Straub, L. Dominguez, J.-E. Shea, N.V. Dokholyan, A. De Simone, B. Ma, R. Nussinov, S. Najafi, S.T. Ngo, A. Loquet, M. Chiricotto, P. Ganguly, J. McCarty, M.S. Li, C. Hall, Y. Wang, Y. Miller, S. Melchionna, B. Habenstein, S. Timr, J. Chen, B. Hnath, B. Strodel, R. Kayed, S. Lesné, G. Wei, F. Sterpone, A.J. Doig, P. Derreumaux, Amyloid oligomers: a joint experimental/computational perspective on alzheimer's disease, Parkinson's disease, type II diabetes, and amyotrophic lateral sclerosis, Chem. Rev. 121 (2021) 2545–2647, https://doi.org/10.1021/acs.chemrev.0c01122.
[13] G. Meisl, X. Yang, E. Hellstrand, B. Frohm, J.B. Kirkegaard, S.I.A. Cohen, C. M. Dobson, S. Linse, T.P.J. Knowles, Differences in nucleation behavior underlie the contrasting aggregation kinetics of the Aβ40 and Aβ42 peptides, Proc. Natl. Acad. Sci. USA 111 (2014) 9384–9389, https://doi.org/10.1073/pnas.1401564111.
[14] F. Chiti, C.M. Dobson, Protein misfolding, amyloid formation, and human disease: a summary of progress over the last decade, Annu. Rev. Biochem. 86 (2017) 27–68, https://doi.org/10.1146/annurev-biochem-061516-045115.
[15] W. Zheng, M.-Y. Tsai, P.G. Wolynes, Comparing the aggregation free energy landscapes of amyloid beta(1–42) and amyloid beta(1–40), J. Am. Chem. Soc. 139 (2017) 16666–16676, https://doi.org/10.1021/jacs.7b08089.
[16] C.E. Heo, T.S. Choi, H.I. Kim, Competitive homo- and hetero- self-assembly of amyloid-β 1–42 and 1–40 in the early stage of fibrillation, Int. J. Mass Spectrom. Ion Process. 428 (2018) 15–21, https://doi.org/10.1016/j.ijms.2018.02.002.
[17] G. Festa, F. Mallamace, G.M. Sancesario, C. Corsaro, D. Mallamace, E. Fazio, L. Arcidiacono, V. Garcia Sakai, R. Senesi, E. Preziosi, G. Sancesario, C. Andreani, Aggregation states of aβ1–40, aβ1–42 and aβp3–42 amyloid beta peptides: a sans study, Int. J. Mol. Sci. 20 (2019) 4126, https://doi.org/10.3390/ijms20174126.
[18] P.N. Nirmalraj, J. List, S. Battacharya, G. Howe, L. Xu, D. Thompson, M. Mayer, Complete aggregation pathway of amyloid β (1-40) and (1-42) resolved on an atomically clean interface, Sci. Adv. 6 (2020) eaaz6014, https://doi.org/10.1126/sciadv.aaz6014.
[19] L. Wang, K. Eom, T. Kwon, Different aggregation pathways and structures for Aβ40 and Aβ42 peptides, Biomolecules 11 (2021) 198, https://doi.org/10.3390/biom11020198.
[20] M. Deleanu, J.-F. Hernandez, L. Cipelletti, J.-P. Biron, E. Rossi, M. Taverna, H. Cottet, J. Chamieh, Unraveling the speciation of β-amyloid peptides during the aggregation process by taylor dispersion analysis, Anal. Chem. 93 (2021) 6523–6533, https://doi.org/10.1021/acs.analchem.1c00527.
[21] M. Deleanu, O. Deschaume, L. Cipelletti, J.-F. Hernandez, C. Bartic, H. Cottet, J. Chamieh, Taylor dispersion analysis and atomic force microscopy provide a quantitative insight into the aggregation kinetics of Aβ (1–40)/aβ (1–42) amyloid peptide mixtures, ACS Chem. Neurosci. 13 (2022) 786–795, https://doi.org/10.1021/acschemneuro.1c00784.
[22] G.A. Braun, A.J. Dear, K. Sanagavarapu, H. Zetterberg, S. Linse, Amyloid-β peptide 37, 38 and 40 individually and cooperatively inhibit amyloid-β 42 aggregation, Chem. Sci. 13 (2022) 2423–2439, https://doi.org/10.1039/D1SC02990H.
[23] S.G. Itoh, M. Yagi-Utsumi, K. Kato, H. Okumura, Key residue for aggregation of amyloid-β peptides, ACS Chem. Neurosci. 13 (2022) 3139–3151, https://doi.org/10.1021/acschemneuro.2c00358.
[24] P. Dey, P. Biswas, Exploring the aggregation of amyloid-β 42 through Monte Carlo simulations, Biophys. Chem. 297 (2023) 107011, https://doi.org/10.1016/j.bpc.2023.107011.
[25] M. Juković, I. Ratkaj, D. Kalafatovic, N.J. Bradshaw, Amyloids, amorphous aggregates and assemblies of peptides - assessing aggregation, Biophys. Chem. 308 (2024) 107202, https://doi.org/10.1016/j.bpc.2024.107202.
[26] W. Yong, A. Lomakin, M.D. Kirkitadze, D.B. Teplow, S.H. Chen, G.B. Benedek, Structure determination of micelle-like intermediates in amyloid beta -protein fibril assembly by using small angle neutron scattering, Proc. Natl. Acad. Sci. U. S. A 99 150–154. https://doi.org/10.1073/pnas.012584899.
[27] R.D. Johnson, J.A. Schauerte, K.C. Wisser, A. Gafni, D.G. Steel, Direct observation of single amyloid-β(1-40) oligomers on live cells: binding and growth at physiological concentrations, PLoS One 6 (2011) e23970, https://doi.org/10.1371/journal.pone.0023970.
[28] S. Nag, B. Sarkar, A. Bandyopadhyay, B. Sahoo, V.K.A. Sreenivasan, M. Kombrabail, C. Muralidharan, S. Maiti, Nature of the amyloid-β monomer and the monomer-oligomer equilibrium, J. Biol. Chem. 286 (2011) 13827–13833, https://doi.org/10.1074/jbc.M110.199885.
[29] B. Morel, M.P. Carrasco, S. Jurado, C. Marco, F. Conejero-Lara, Dynamic micellar oligomers of amyloid beta peptides play a crucial role in their aggregation mechanisms, Phys. Chem. Chem. Phys. 20 (2018) 20597–20614, https://doi.org/10.1039/C8CP02685H.
[30] Y. Lin, B.R. Sahoo, D. Ozawa, M. Kinoshita, J. Kang, M.H. Lim, M. Okumura, Y. H. Huh, E. Moon, J.H. Jang, H.-J. Lee, K.-Y. Ryu, S. Ham, H.-S. Won, K.-S. Ryu, T. Sugiki, J.K. Bang, H.-S. Hoe, T. Fujiwara, A. Ramamoorthy, Y.-H. Lee, Diverse structural conversion and aggregation pathways of Alzheimer's amyloid-β (1–40), ACS Nano 13 (2019) 8766–8783, https://doi.org/10.1021/acsnano.9b01578.
[31] L.G. Sharma, L.M. Pandey, Shear-induced aggregation of amyloid β (1–40) in a parallel plate geometry, J. Biomol. Struct. Dyn. 39 (2021) 6415–6423, https://doi.org/10.1080/07391102.2020.1798814.
[32] A. Das, A. Gupta, Y. Hong, J.A. Carver, S. Maiti, A spectroscopic marker for structural transitions associated with amyloid-β aggregation, Biochemistry 59 (2020) 1813–1822, https://doi.org/10.1021/acs.biochem.0c00113.
[33] M. Novo, S. Freire, W. Al-Soufi, Critical aggregation concentration for the formation of early Amyloid-β (1-42) oligomers, Sci. Rep. 8 (2018) 1783, https://doi.org/10.1038/s41598-018-19961-3.
[34] M. Novo, C. Pérez-González, S. Freire, W. Al-Soufi, Early aggregation of amyloid-β(1–42) studied by fluorescence correlation spectroscopy, in: A.S. Cieplak (Ed.), Protein Aggreg, Springer US, New York, NY, 2023, pp. 1–14, https://doi.org/10.1007/978-1-0716-2597-2_1.
[35] J.R. Brender, J. Krishnamoorthy, M.F. Sciacca, S. Vivekanandan, L. D'Urso, J. Chen, C. La Rosa, A. Ramamoorthy, Probing the sources of the apparent irreproducibility of amyloid formation: drastic changes in kinetics and a switch in mechanism due to micellelike oligomer formation at critical concentrations of IAPP, J. Phys. Chem. B 119 (2015) 2886–2896, https://doi.org/10.1021/jp511758w.
[36] B. Morel, M.P. Carrasco-Jiménez, S. Jurado, F. Conejero-Lara, Rapid conversion of amyloid-beta 1-40 oligomers to mature fibrils through a self-catalytic bimolecular process, Int. J. Mol. Sci. 22 (2021) 6370, https://doi.org/10.3390/ijms22126370.
[37] S. Amin, G.V. Barnett, J.A. Pathak, C.J. Roberts, P.S. Sarangapani, Protein aggregation, particle formation, characterization & rheology, Curr. Opin. Colloid Interface Sci. 19 (2014) 438–449, https://doi.org/10.1016/j.cocis.2014.10.002.
[38] W.B. Stine, L. Jungbauer, C. Yu, M.J. Ladu, Preparing synthetic Aβ in different aggregation states, Methods Mol. Biol. Clifton NJ 670 (2011) 13–32, https://doi.org/10.1007/978-1-60761-744-0_2.
[39] W.B. Stine, K.N. Dahlgren, G.A. Krafft, M.J. LaDu, In vitro characterization of conditions for amyloid-beta peptide oligomerization and fibrillogenesis, J. Biol. Chem. 278 (2003) 11612–11622, https://doi.org/10.1074/JBC.M210207200.
[40] J. Bordello, M. Novo, W. Al-Soufi, Exchange-dynamics of a neutral hydrophobic dye in micellar solutions studied by Fluorescence Correlation Spectroscopy, J. Colloid Interface Sci. 345 (2010) 369–376, https://doi.org/10.1016/J.JCIS.2010.01.064.
[41] D. Granadero, J. Bordello, M.J. Pérez-Alvite, M. Novo, W. Al-Soufi, Host-guest complexation studied by fluorescence correlation spectroscopy: adamantane–cyclodextrin inclusion, Int. J. Mol. Sci. 11 (2010) 173–188, https://doi.org/10.3390/IJMS11010173.
[42] M. Novo, S. Felekyan, C.A.M. Seidel, W. Al-Soufi, Dye-exchange dynamics in micellar solutions studied by fluorescence correlation spectroscopy, J. Phys. Chem. B 111 (2007) 3614–3624, https://doi.org/10.1021/jp0657639.
[43] Z. Petrášek, P. Schwille, Precise measurement of diffusion coefficients using scanning fluorescence correlation spectroscopy, Biophys. J. 94 (2008) 1437–1448, https://doi.org/10.1529/biophysj.107.108811.
[44] P.-O. Gendron, F. Avaltroni, K.J. Wilkinson, Diffusion coefficients of several rhodamine derivatives as determined by pulsed field gradient–nuclear magnetic resonance and fluorescence correlation spectroscopy, J. Fluoresc. 18 (2008) 1093–1101, https://doi.org/10.1007/s10895-008-0357-7.
[45] W. Al-Soufi, L. Piñeiro, M. Novo, A model for monomer and micellar concentrations in surfactant solutions: application to conductivity, NMR, diffusion, and surface tension data, J. Colloid Interface Sci. 370 (2012) 102–110, https://doi.org/10.1016/j.jcis.2011.12.037.
[46] J. Danielsson, J. Jarvet, P. Damberg, A. Graslund, Translational diffusion measured by PFG-NMR on full length and fragments of the Alzheimer Ab(1-40) peptide. Determination of hydrodynamic radii of random coil peptides of varying length, Magn. Reson. Chem. 40 (2002) S89–S97.
[47] J.P. Leite, A. Gimeno, P. Taboada, J.J. Jiménez-Barbero, L. Gales, Dissection of the key steps of amyloid-β peptide 1–40 fibrillogenesis, Int. J. Biol. Macromol. 164 (2020) 2240–2246, https://doi.org/10.1016/j.ijbiomac.2020.08.023.